
TWINCHER: BIJECTIVE REPRESENTATION LEARNING FOR ROBUST INVERSION OF CONTINUOUS SYSTEMS

Arkady Gonoskov

Department of Physics, University of Gothenburg, SE-41296 Gothenburg, Sweden
arkady.gonoskov@physics.gu.se

May 14, 2026

ABSTRACT

Recent advances in AI have been primarily driven by large-scale neural architectures that excel at function approximation, rather than by tailored inductive biases and inference or learning strategies that could be important for resource-efficient real-world perception and planning through the solution of inverse problems. In this work, we consider the possibility of enabling robust inversion of continuous forward processes $p \mapsto y$ by learning representations of y that are bijectively aligned with p while remaining insensitive to perturbations in y caused by noise or model mismatch. We propose Twincher, a class of architectures based on stacks of structured diffeomorphic transformations and tailored adversarial training strategies that enable learning such bijective representations. We provide a public API for training and inference and empirically demonstrate the ability of the proposed architecture to efficiently learn bijective representations of synthetic systems, thereby enabling robust and efficient iterative inverse inference. Compared to a baseline inverse-modeling approach, the method exhibits improved data efficiency and robustness, providing initial evidence for the potential of bijective representation learning in robotics, vision, and physical AI.

Keywords Bijective representation learning · representation learning · inverse problems · robust inverse inference · active learning · robotics · physical AI

1 Introduction

The overwhelming majority of contemporary AI systems are built upon highly parameterized function approximators composed of simple repeated computational units, typically affine transformations followed by pointwise nonlinearities, trained via gradient-based optimization on large-scale datasets. While scale in both data and model capacity has been a key driver of recent progress [1], it is widely recognized that generalization depends critically on the inductive biases encoded in model architectures. Canonical examples include weight sharing in convolutional networks [2], compositional structure in deep hierarchies, and relational reasoning via attention mechanisms in Transformer architectures [3]. More broadly, the role of inductive bias in enabling efficient learning has been emphasized across many domains (see, e.g., Refs. [4, 5]). Furthermore, there is increasing recognition that AI systems operating in real-world interactive environments can benefit from the joint consideration of inductive bias and structured representation learning that can leverage adaptive experimentation and multi-step inference (see, e.g., Refs. [6–12]).

More broadly, structured representation learning combined with tailored inductive biases and tailored active learning strategies may play an important role across several evolving paradigms for physical AI systems, including model-based learning [13, 14], vision-language and vision-language-action foundation models [15–17], direct policy learning [18–21], and structured perception–planning–control architectures. In many such settings, partial knowledge of the forward process may be available through physics-based simulators, learned surrogate models, differentiable renderers, or interaction with the environment itself. A central challenge then becomes how to construct compact and resource-efficient representations of the observable space that are sufficiently informative to support robust inversion, uncertainty-aware inference, and navigation in the space of controllable system states. This naturally motivates the problem of learning structured representations to support robust system inversion as a first step.

Motivated by this perspective, we study the problem of learning representations of system outputs that are bijectively aligned with their corresponding inputs, while also being encouraged to be robust to perturbations arising from noise or model mismatch. This problem referred hereafter as *bijective representation learning* can be viewed as a structured and inference-oriented extension of the approximate bijective correspondence [22]. We introduce Twincher, a class of scalable invertible diffeomorphic transformations as structured computational primitives for learning and interacting with continuous or partially continuous black-box systems of the form $y = f(p)$. In contrast to standard normalizing flow architectures such as RealNVP [23] and Glow [24], which primarily target flexible density estimation, our construction couples the design of the computational primitive with a training strategy explicitly aimed at inducing stable and invertible representations for inverse inference.

For a broad class of well-behaved forward mappings f , characterized by bounded and non-degenerate Jacobians over $p \in [-1, 1]^{n_p}$, the proposed approach gives rise – under sufficient model capacity – to a latent subspace $u \in U \subset \mathbb{R}^{n_p}$ that forms a bijective reparameterization of p . Concretely, the learned mapping satisfies $u(y(p)) \leftrightarrow p$, such that u serves as an invertible coordinate system for the generative factors. This property is not imposed analytically, but emerges from the joint architectural constraints and training procedure, and is consistently observed across a wide range of synthetic black-box systems.

In parallel, the training objective promotes local invariance of u to perturbations in observation space, e.g., via adversarial exposure to mismatched inputs, leading to representations that satisfy $u(y) \approx u(y + y_{\text{mismatch}})$ over a controlled range of deviations. This combination of invertibility and stability directly impacts the conditioning of the inverse problem. In particular, it induces a regime in which the inference error scales proportionally to perturbations in y , $|p_{\text{inferred}} - p_{\text{true}}| < \eta |y_{\text{mismatch}}|$, where η reflects the local sensitivity of the inferred inverse and can be actively minimized during training through targeted exploration of worst-case perturbations. Empirically, this leads to a reproducible reduction of η with increasing model capacity and training coverage, enabling fast and well-conditioned iterative inversion using the latent domain \mathcal{U} .

More broadly, the proposed framework can be viewed as a general approach to both perception and action planning in continuous real-world systems through exploration of their digital twins, whether learned surrogates or physics-based simulators, such as vision renderers. In this setting, the learned robust bijective representation serves as a compact and resource-efficient structure that is sufficient for fast inverse inference as well as navigation through the space of feasible system states. This makes the approach particularly relevant for settings in which perception and action are tightly coupled, including vision-based system identification, robotics, and broader physical AI applications. Beyond these domains, the results suggest that revisiting the choice of underlying computational primitives, rather than relying solely on scaling existing architectures, may provide a complementary path toward improving data efficiency, robustness, and interpretability in modern AI systems.

This paper introduces a novel architectural and training framework for bijective representation learning and inversion in continuous black-box systems. The main contributions are as follows:

- **Structured invertible computational primitives.** We propose a class of scalable diffeomorphic transformations as an alternative to standard architectures based on pointwise nonlinear units. These are explicitly designed to provide inductive bias that learning representations bijectively aligned with underlying generative parameters.
- **Emergent bijective latent parameterization.** We show that, for a broad class of well-behaved forward mappings, the proposed architecture gives rise – under sufficient model capacity – to a latent subspace u that forms a bijective reparameterization of the generative factors p . This property is not analytically imposed, but emerges from the interaction between architectural constraints and the training procedure.
- **Robust inverse inference via stability-inducing training.** We introduce a training strategy that promotes local invariance of the latent representation to perturbations in observation space, yielding improved conditioning of the inverse inference. As a result, we empirically observe that inference error scales proportionally with observation perturbations, with a sensitivity coefficient that can be actively minimized during training.
- **Active learning through sensitivity-driven exploration.** We demonstrate that the learned representation naturally supports an active learning paradigm in which data acquisition is guided by worst-case sensitivity in latent space. This enables systematic reduction of inversion error and improves data efficiency in partially observed continuous systems.

2 Related work

With respect to learning strategies, our approach is related to a class of methods that perform adversarial or worst-case perturbation-based learning, where training dynamics are shaped by gradient-driven construction of challenging

inputs. Representative examples include the Fast Gradient Sign Method (FGSM) [25] and Projected Gradient Descent (PGD) [26], which have been widely studied in the context of adversarial robustness. These approaches can also be interpreted within the broader framework of Distributionally Robust Optimization, where the objective is to improve performance under worst-case shifts in the input distribution [27].

In contrast to these methods, which primarily concern observation space, our method is more closely related to approaches that explicitly structure latent representations. In this context, our work can be related to variational representation learning methods such as β -VAEs [28] and related latent-variable models [29–37] also considered in diffusion-based generative modeling [38] and other problems [39] that can benefit from improved latent space structure and data-efficiency.

A relevant line of work considers the enforcement of invariances or structural constraints in observation and/or representation space. This includes methods that promote invariance to semantically preserving transformations [40, 41], as well as approaches that incorporate topological or geometric structure into learned representations [42–45]. More recent work has explored geometry-inspired regularization directly in latent space to improve representation structure and robustness [46].

With respect to computational primitives, our work relates to a growing line of research that explores alternatives to standard MLP-based architectures by employing parameterized nonlinear functions introducing inductive biases that lead to useful emergent properties. Representative examples include Kolmogorov-Arnold Networks (KANs) [47], spline-based neural networks such as ExSpliNet [48], and Tensor Product Neural Networks (TPNNs) [49], which demonstrate that modifying the functional form of elementary building blocks can lead to improved interpretability, compositionality, or generalization.

In contrast to these approaches, which primarily focus on expressivity and structural decomposition, our construction is based on parameterized diffeomorphic transformations designed to induce invertible and geometrically structured mappings between control and latent spaces. In this sense, it is most closely related to parameterized geometric transformation models such as Continuous Piecewise-Affine-Based (CPAB) transforms [50] and architectures used for normalizing flows, including Non-linear Independent Component Estimation (NICE) [51], real-valued non-volume preserving (realNVP) transformations [23] and GLOW [24].

The outlined approaches highlight the benefits of incorporating explicit inductive bias into representation learning, but typically do not jointly address the interplay between latent structure, invertibility, and active, sensitivity-driven data acquisition. The present work aims to explore this intersection by developing a framework in which these aspects are integrated within a unified representation learning paradigm.

3 Method

Problem setting. Let $p \in \mathcal{P} \subset \mathbb{R}^{n_p}$ denote the primary parameters of interest and $\nu \in \mathcal{N}$ denote nuisance variables capturing noise and model mismatch. Observations are generated by an unknown forward process

$$y = f(p, \nu), \quad y \in \mathcal{Y} \subset \mathbb{R}^{n_y}, \quad (1)$$

where f is treated as a black-box function. The primary objective is to infer p from observations y while remaining robust to variations in ν .

Twincher transformation. We introduce a parametric invertible mapping, denoted *Twincher*:

$$T_\theta : \mathcal{Y} \rightarrow \mathcal{U} \times \mathcal{H}, \quad (u, h) = T_\theta(y), \quad (2)$$

where $u \in \mathcal{U} \subset \mathbb{R}^{n_p}$ is a distilled latent variable and $h \in \mathcal{H}$ is a residual latent variable such that $n_p + n_h = n_y$ (hereafter we denote $n_{(\cdot)} := \dim(\cdot)$). The mapping T_θ is constructed as a composition of n_ℓ transformations

$$T_\theta = \tau_{n_\ell} \circ \cdots \circ \tau_1, \quad (3)$$

where each τ_i is a parameterized, diffeomorphic transformation.

Inverse inference using latent space. The transformation T_θ is trained to induce a structured decomposition of the observation space such that the mapping between p and u becomes bijective under suitable conditions on f and sufficient model capacity. Reaching the bijection between p and u can enable a globally convergent iterative solution of the inverse problem. Given a target observation y^* , inference is performed by first computing $(u^*, h^*) = T_\theta(y^*)$ and then solving

$$p^* = \arg \min_p \|u(f(p, \nu_0)) - u^*\|^2, \quad (4)$$

where ν_0 is a nominal or sampled nuisance configuration. Due to the learned structure of u , this optimization is well-conditioned and can be efficiently solved using iterative methods such as Gauss–Newton.

Robustness to nuisance variables. To promote invariance with respect to nuisance variations, the representation u is encouraged to satisfy

$$u(f(p, \nu)) \approx u(f(p, \nu + \delta\nu)), \quad (5)$$

for admissible perturbations $\delta\nu$. This property is enforced through a training strategy based on adversarial or worst-case perturbations in observation space.

Remark. The residual variable h captures variability in y that is not required for recovering p , and may optionally be used for generative modeling or uncertainty characterization.

Model class and training strategies. The Twincher framework defines a broad class of architectures constructed as compositions of parameterized diffeomorphic transformations, including but not limited to multi-dimensional CPAB transforms, RealNVP, GLOW, and related invertible models. Rather than prescribing a specific parameterization, the framework is characterized by the following structural requirements:

1. **Robust invertibility:** the transformation T_θ is constructed such that its Jacobian determinant is uniformly bounded away from zero,

$$\left| \det \left(\frac{\partial z}{\partial y} \right) \right| \geq \epsilon > 0, \quad (6)$$

ensuring that invertibility is preserved for all admissible parameter values;

2. **Differentiability:** the mapping T_θ depends continuously and differentially on its parameters θ ;
3. **Expressivity:** the model class is sufficiently expressive to approximate complex transformations, including nontrivial permutations and structured rearrangements of the input space.

Training within this framework is coupled with active or adversarial data generation and aims to jointly promote (i) bijective alignment between p and u , and (ii) invariance of u with respect to nuisance variables ν .

Bijectivity-promoting objectives. Several strategies can be employed to encourage bijectivity of the mapping $p \leftrightarrow u(f(p, \nu))$. One approach is to promote a co-Lipschitz condition of the form

$$\|u(f(a, \nu)) - u(f(b, \nu))\| \geq M \|a - b\|, \quad \forall a, b \in \mathcal{P}, \quad (7)$$

with $M > 0$. In practice, pairs (a, b) can be selected or adversarially optimized to identify near-violations of this condition, while the model parameters θ are updated to increase the effective margin M . Alternative formulations include minimizing the probability of collapse events,

$$\mathbb{P}(\|u(f(a, \nu)) - u(f(b, \nu))\| < M \|a - b\|), \quad (8)$$

as well as incorporating geometric regularization techniques that promote well-conditioned embeddings, such as reach-based constraints [46].

Robustness-promoting objectives. Robustness with respect to nuisance variables can be encouraged through adversarial perturbations that target the sensitivity of u to variations in ν . In particular, one may consider perturbations $\delta\nu$ that maximize the induced change in u ,

$$\delta u = \frac{\partial u}{\partial y} \frac{\partial y}{\partial \nu} \delta \nu, \quad (9)$$

while simultaneously updating θ to minimize $\|\delta u\|$. This can be extended by jointly exploring perturbations in both ν and p , leading to a worst-case sensitivity analysis over the joint space of nuisance and primary variables.

Implementation considerations. In practice, the Twincher framework admits a range of architectural and training instantiations. We explored several such configurations on synthetic test problems, with a focus on understanding factors that influence convergence toward bijective latent representations. Our empirical findings indicate that the choice of computational primitives plays a critical role in avoiding suboptimal local minima, and that appropriately tailored parameterizations can significantly improve training stability and performance, suggesting the presence of a beneficial inductive bias for this class of problems.

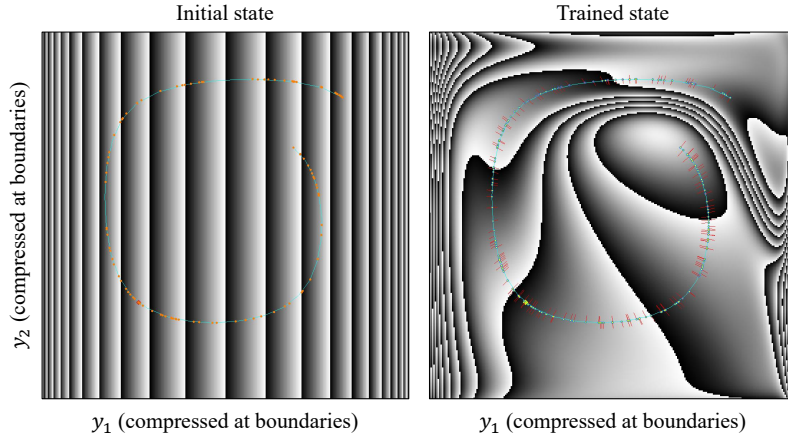


Figure 1: Learning a bijective mapping from a one-dimensional parameter along a spiral (blue line) into two-dimensional space. The images show the value of u_1 (repeated grayscale) as a function of y_1 and y_2 (non-linear scale compressed near boundaries) before training (left) and after training (right).

Elemental example We illustrate the concept using a simple example: learning a bijective representation for a forward problem in which a one-dimensional parameter along a spiral is mapped into two-dimensional space, as shown by the blue line in Fig. 1 (left), i.e., $n_p = n_u = 1, n_y = 2$. The figure shows the sole component of u_1 as a function of y_1 and y_2 (nonlinear scale; compressed near boundaries), with repeated grayscale used for improved visibility. Sharp black-to-white transitions indicate iso-value contours. Before training (left), some contours intersect the spiral more than once, indicating that the mapping is not bijective. After training (right), all contours intersect the spiral exactly once, demonstrating that a bijective mapping has been successfully learned. The robustness of the representation corresponds to the observation that the contours cross the spiral nearly perpendicularly.

4 Experimental Results

To ensure the reproducibility of the results presented, we provide access to a public API [52] for both training and inference (through query loops). This API enables independent researchers to reproduce all experiments reported in this work, as well as to evaluate the approach on new tasks.

4.1 Learning bijective representations in the noise-free setting

We begin by evaluating the ability of the proposed architecture to construct bijective latent representations in the simplest setting, namely static random sampling of the training set at initiation. In this regime, data for training a Twincher model consists of randomly sampled points together with local Jacobian estimates of the forward process.

Harmonic entangler. As a controlled benchmark family, we introduce a class of synthetic black-box functions $y = f(p)$, referred to as *harmonic entanglers*, designed to generate nonlinear yet fully invertible mappings of tunable complexity.

The construction starts by embedding the input vector $p \in [-1, 1]^{n_p}$ into a higher-dimensional state vector

$$s_0 = (p, s_{n_p+1}^{\text{pad}}, \dots, s_{n_s}^{\text{pad}}), \tag{10}$$

where the padding components $s_i^{\text{pad}} \sim U(-1, 1)$ are sampled once at initialization to match the target dimensionality $n_s = n_y$.

The forward mapping is then constructed as a composition of e_n invertible layers

$$s_0 \rightarrow s_1 \rightarrow \dots \rightarrow s_{e_n}, \tag{11}$$

with the final observation defined as $y = s_{e_n}$. At each layer, the current state vector is split into two equal parts,

$$s_i = (x_1, x_2), \tag{12}$$

assuming even n_s . Two coupling transformations inspired by the RealNVP architecture are then applied:

$$y_1 = x_1, \tag{13}$$

$$y_2 = x_2 \odot \exp(\sigma_y(x_1)) + \tau_y(x_1), \tag{14}$$

$$z_2 = y_2, \tag{15}$$

$$z_1 = y_1 \odot \exp(\sigma_z(y_2)) + \tau_z(y_2), \tag{16}$$

where \odot denotes element-wise multiplication.

To prevent uncontrolled growth of s components during sequential application of layers' transformations, each component is subsequently normalized through the invertible mapping

$$z^{(j)} \rightarrow \frac{z^{(j)}}{\sqrt{1 + (z^{(j)})^2}}, \tag{17}$$

which smoothly maps values to the interval $(-1, 1)$. The output vector s_{i+1} is then formed by applying a fixed random permutation to the concatenated components of (z_1, z_2) .

The functions $\sigma_y, \tau_y, \sigma_z,$ and τ_z are modeled as independent harmonic operators. For an input vector $\mathbf{x} \in \mathbb{R}^{n_s/2}$, the j -th output component is defined as

$$\text{out}_j(\mathbf{x}) = \frac{2}{n_s} \sum_{k=1}^{n_s/2} \sin(w_{jk}x_k + b_{jk}), \tag{18}$$

where

$$w_{jk} \sim U(-\pi w_{\text{amp}}, \pi w_{\text{amp}}), \quad b_{jk} \sim U(-\pi, \pi) \tag{19}$$

are fixed random coefficients sampled independently at initialization.

The parameter w_{amp} controls the complexity of the generated mapping: larger values induce higher-frequency modulation and therefore stronger nonlinear entanglement between latent dimensions. Unless stated otherwise, the experiments below use $n_p = 2, n_s = 4,$ and $e_n = 3,$ while varying $w_{\text{amp}} \in [0.5, 1.5].$

As a measure of problem complexity, we use

$$C := -\log(p_{\text{rand}}^{\text{success}}), \tag{20}$$

where $p_{\text{rand}}^{\text{success}}$ is the probability that a randomly sampled point $p_{\text{in}} \sim U([-1, 1]^{n_p})$ lies within the convergence basin of another randomly sampled target $p^* \sim U([-1, 1]^{n_p})$ under L^2 descent in \mathcal{Y} . In other words, it quantifies the likelihood that gradient-based descent from a random initialization converges to the correct solution. In practice, we estimate $p_{\text{rand}}^{\text{success}}$ empirically over a large set of trial tasks using a clipped-step Gauss–Newton method.

In Fig. 2, we show the empirically estimated values of C for an example of a randomly generated harmonic entangler with three different values of w_{amp} . The forward mapping is visualized by a grid spanning the $p \in [-1, 1]^2$ domain in the space of $(y_1, y_2, y_3),$ with the fourth coordinate represented by color.

Test problem formulation. We consider the problem of learning to iteratively solve inverse problems for a given instance of a harmonic entangler $y = E(p)$ generated using randomly initialized parameters $w_{jk}, b_{jk},$ and s^{pad} . The *learner* is first allowed to explore the provided instance E by querying the forward transform at arbitrary points $p,$ subject to a fixed query budget referred to as the *number of queries* or n_{calls} . After the exploration phase, the learner is presented with a large test batch of target vectors y_i^{true} generated from undisclosed parameters $p_i^{\text{true}} \sim U([-1, 1]^2)$. The task is to iteratively produce estimates p_i^{trial} such that $E(p_i^{\text{trial}})$ matches y_i^{true} as closely as possible. At iteration zero, the estimate p_i^{trial} must be inferred solely from y_i^{true} . Each subsequent iteration may additionally use $n_p + 1$ evaluations of the forward transform per test instance in order to evaluate $y(p_i^{\text{trial}})$ and the Jacobian $\partial y / \partial p$ at the current point.

Baseline learner: MLP + Gauss-Newton. To assess the capability of the presented method we compare its performance on the described test problem with that of a baseline learner. For the baseline method we choose a composition of multilayer perceptron (MLP) for generating the zeroth p_i^{trial} and a clipped Gauss-Newton iterator in the space \mathcal{Y} for iterative refinement.

Exploration phase. The training dataset is formed by drawing n_{calls} points $p_i^{\text{TS}} \sim \mathcal{U}([-1, 1]^{n_p})$ uniformly at random and evaluating $y_i^{\text{TS}} = E(p_i^{\text{TS}}),$ exhausting the full query budget in a single passive pass with no feedback-driven selection.

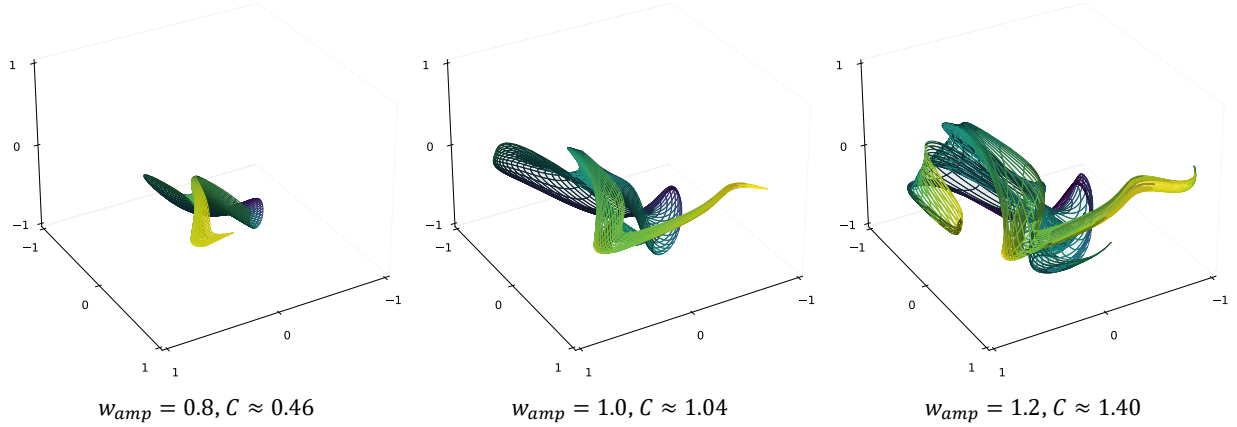


Figure 2: Examples of a harmonic entangler for three values of w_{amp} and the corresponding estimated problem complexity C . The forward mapping is shown as a grid spanning the $p \in [-1, 1]^2$ domain in the (y_1, y_2, y_3) space, with the fourth coordinate represented by color.

Model for generating initial proposals. An MLP is trained on the dataset $\{(y_i^{\text{TS}}, p_i^{\text{TS}})\}_{i=1}^{n_{\text{calls}}}$ to approximate the inverse mapping $y \mapsto p$. The network maps $\mathbb{R}^{n_y} \rightarrow \mathbb{R}^{n_p}$ through four fully-connected hidden layers of width 16 with \tanh activations, followed by a scaled output activation $1.5 \tanh(\cdot)$. The 1.5 scaling factor is chosen to guarantee that the target range $[-1, 1]^{n_p}$ is attainable without pushing the pre-activation toward $\pm\infty$, which would cause gradient saturation near the boundaries under a plain \tanh output. For $n_p=2, n_s=4$, this amounts to approximately 1000 trainable parameters. Training minimises mean-squared error via Adam (learning rate 10^{-3}) for up to 1000 epochs; early stopping with a patience of 10 epochs and a 10% held-out validation split is applied when $N \geq 20$ to prevent overfitting.

Iterative refinement. After the exploration phase, the MLP produces an initial estimate $p^{(0)} = \text{MLP}(y^{\text{true}})$ for each test target y^{true} . Each subsequent refinement step uses n_p+1 forward evaluations to compute $y(p^{(t)})$ and the numerical Jacobian

$$J_{ij}^{(t)} = \frac{[E(p^{(t)} + \delta e_j)]_i - [E(p^{(t)})]_i}{\delta}, \quad \delta = 10^{-7}, \quad (21)$$

where e_j is the j -th canonical basis vector. The Gauss-Newton update is then obtained by solving the regularised normal equations

$$(J^\top J + \lambda I) \Delta p = J^\top (y^{\text{true}} - E(p^{(t)})), \quad \lambda = 10^{-3}, \quad (22)$$

with step clipping $\Delta p \leftarrow \Delta p \min(1, \Delta_{\text{max}}/\|\Delta p\|)$ ($\Delta_{\text{max}}=0.1$) to prevent overshooting the domain of expected valid approximation of Jacobian, and the update is projected back into the feasible domain: $p^{(t+1)} = \text{clip}(p^{(t)} + \Delta p, -1, 1)$.

Twincher test model. For the basic implementation of the Twincher learner, we use a 64-layer architecture with approximately 1000 trainable parameters, matching the capacity of the baseline model. During the exploration phase, forward evaluations are performed at randomly sampled points within the available query budget.

If the training results in the construction of a bijective representation, an auxiliary MLP is trained to approximate the mapping $u \mapsto p$, which is subsequently used to generate the initial trails $p^{(0)}$. The MLP architecture is close to that of the MLP used in the baseline model. Iterative refinement is then performed analogously to the baseline approach, except that the optimization is carried out in the \mathcal{U} representation space rather than directly in \mathcal{Y} .

Results for harmonic entangler. Figure 3 maps the outcome of learning process for both learners across a range of problem complexities C and query budgets n_{calls} . Each point corresponds to one trial: a harmonic entangler is drawn at random, its complexity C is estimated independently as described above, and the learner is granted a budget of n_{calls} queries during the exploration phase. After exploration, performance is evaluated on a batch of 10^3 test tasks with targets y_i^{true} sampled uniformly from $[-1, 1]^2$. A trial is declared a *success* if the largest (worst-case) residual after five refinement steps satisfies

$$\max_i \|E(p_i^{(5)}) - y_i^{\text{true}}\| < 10^{-2}, \quad (23)$$

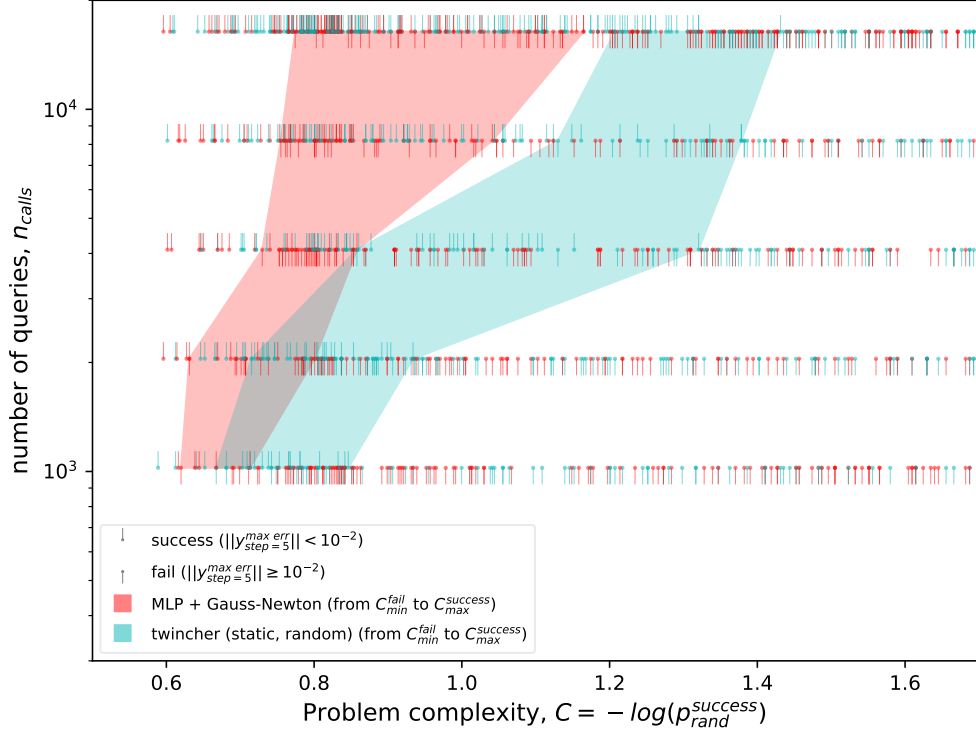


Figure 3: Learning outcome as a function of problem complexity C and query budget n_{calls} for the MLP+Gauss-Newton baseline and the twincer learner. Each point is one trial on a randomly drawn harmonic entangler; an upward tick denotes success ($\max_i \|E(p_i^{(5)}) - y_i^{\text{true}}\| < 10^{-2}$) and a downward tick denotes failure. The shaded band for each learner spans the transition region at each budget level: from the smallest C at which a failure was observed (left edge) to the largest C at which a success was observed (right edge).

and a *failure* otherwise. Successful trials are marked with an upward tick; failures with a downward tick.

For each learner, the shaded band delineates the transition region in the (C, n_{calls}) plane: its left edge is the smallest C at which a failure was observed for the given budget n_{calls} , and its right edge is the largest C at which a success was observed. Points lying to the left of the band correspond to problems that were consistently solved at that budget, while points to the right were consistently failed.

The Twincer model begins to systematically outperform the MLP+Gauss-Newton baseline at approximately $n_{\text{calls}} \approx 4000$. This improvement is enabled by the successful construction of a bijective representation. Increasing the query budget further extends the range of problem complexities for which successful inversion is achieved. The change in trend observed near $n_{\text{calls}} \approx 8000$ appears to indicate an underparameterization regime: problems with complexity $C > 1.4$ intrinsically require a larger number of learnable parameters to construct an accurate bijective representation.

We now examine in greater detail how the residual error $|E(p_i^{(t)}) - y_i^{\text{true}}|$ decays with refinement step t for trials with $C < 1.0$ and $N \geq 8192$, a regime in which the available budget appears to be sufficient for learning bijective representation (see Fig. 3). Figure 4 shows the worst-case residual $\max_i \|E(p_i^{(t)}) - y_i^{\text{true}}\|$ as a function of refinement step t for every trial in this group; line width increases with C and dash density increases with n_{calls} , so that thicker, denser curves correspond to harder, better-sampled problems. Unlike the baseline method, the twincer learner reduces the residual to near machine precision within just a few refinement steps across all cases, demonstrating that its learned representation enables rapid and globally reliable convergence when solving inverse problems.

Finally, Fig. 5 shows how the worst-case residual after five refinement steps varies with the query budget n_{calls} for all trials with $C < 1.0$. Each scatter point corresponds to an independent trial. Downward-pointing triangles at the lower boundary of the vertical axis indicate budget levels at which a fraction of trials fell below the plotted range; the adjacent percentage label specifies that fraction. Solid lines denote the per-learner mean. The MLP+Gauss-Newton baseline exhibits a systematic power-law reduction of the residual with increasing n_{calls} , consistent with the *compute-efficient*

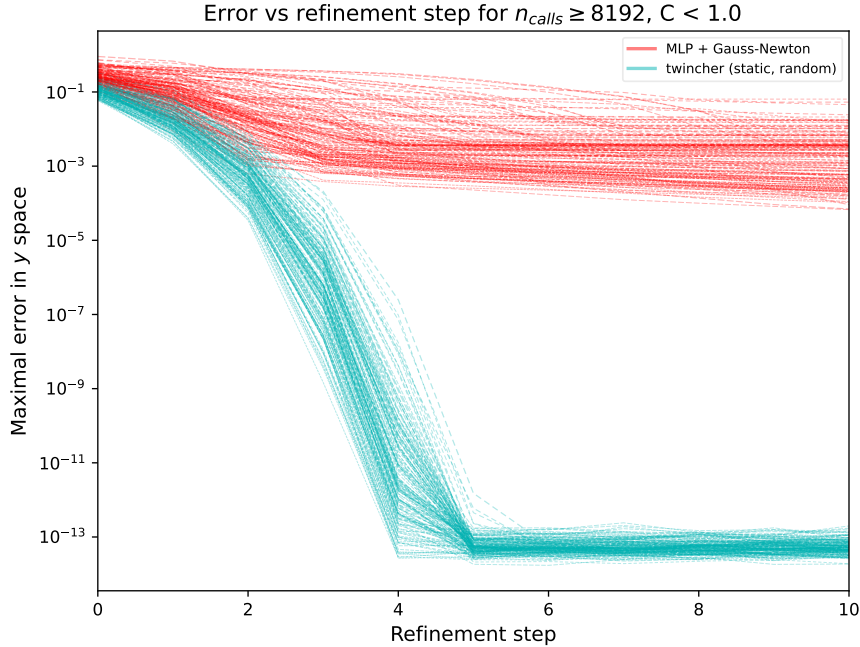


Figure 4: Worst-case residual $\max_i \|E(p_i^{(t)}) - y_i^{\text{true}}\|$ as a function of refinement step t , shown for all trials with $C < 1.0$ and $n_{\text{calls}} \geq 8192$. Each curve is one trial; line width increases with C and dash density increases with $\log_2(N/1024)$.

frontier [1], where prediction error decreases approximately as a power law in dataset size. In contrast, the Twincher learner undergoes a sharp transition by $n_{\text{calls}} = 8192$, at which the residual collapses to near machine precision across all evaluated trials. This behavior deviates markedly from the gradual scaling trend observed for the baseline and suggests that the learned representation enables a qualitatively different inversion regime rather than a purely incremental improvement in approximation accuracy, broadly associated with the compute-efficient frontier [1].

4.2 Inferring 3D parameters from noisy depth maps

In this section, we consider a practical application of the proposed architecture to the problem of inferring parameters of a 3D object from noisy depth maps while maintaining well-controlled error bounds. This setting can be viewed as a prototype virtual metrology system for quality inspection of objects on a conveyor belt observed by a LiDAR sensor, and is also relevant to robotic manipulation tasks.

The forward process is implemented using a 3D renderer that generates depth maps of a hinge composed of two connected parts. The configuration of the hinge is controlled by three parameters ($n_p = 3$). The first parameter specifies the relative angle between the two hinge components and varies within the interval $[-\pi/3, \pi/3]$ to avoid physical self-intersections. The second parameter controls the global orientation of the first hinge component within the range $[-\pi/3, 4\pi/3]$. We intentionally avoid the full rotational range in order to preserve invertibility of the forward problem; in practice, the full range could be covered by training multiple Twincher instances on overlapping angular intervals. The third parameter controls the relative offset between the connection axes of hinge components.

We assume that the hinge remains centered in the observed depth maps. The renderer outputs a 128×128 floating-point depth image in which each pixel intensity represents the distance to the observation point scaled to the interval $[-1, 1]$.

To emulate realistic sensing artifacts, we introduce two sources of noise. First, each pixel intensity is perturbed by additive uniform noise sampled from $U(-0.5, 0.5)$. Second, we introduce occasional directional mismatch artifacts at the pixel level: independently for each spatial coordinate, a pixel is displaced by ± 1 with probability 0.2, causing the recorded intensity to be sampled from a neighboring pixel location. Finally, the resulting image is downsampled to an 8×8 representation by average pooling over non-overlapping 16×16 regions, yielding a 64-dimensional input vector for the Twincher model.

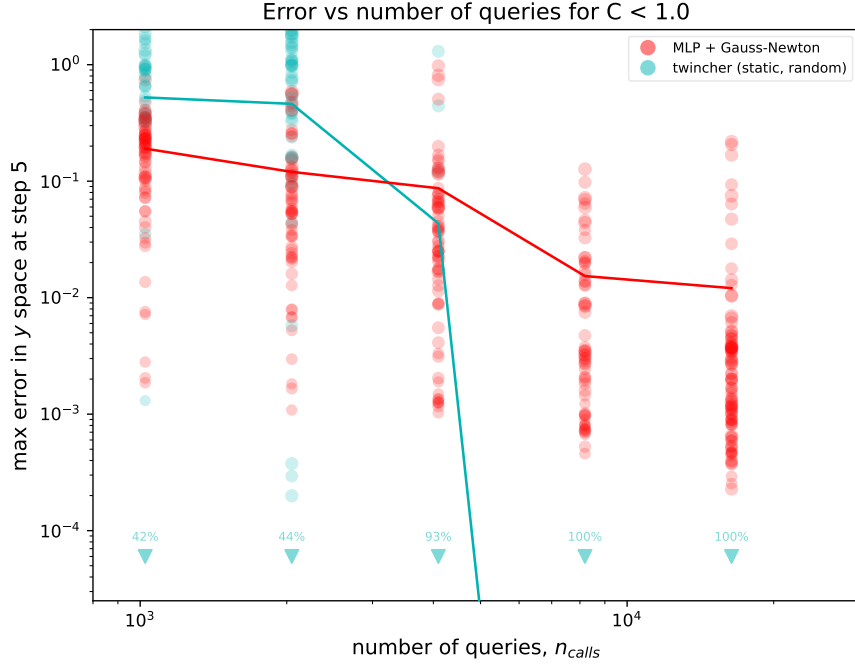


Figure 5: Worst-case residual $\max_i \|E(p_i^{(5)}) - y_i^{\text{true}}\|$ at refinement step 5 as a function of query budget n_{calls} , for all trials with $C < 1.0$; solid lines show the per-learner mean. Downward-pointing triangles at the lower axis boundary indicate budget levels at which a fraction of trials (labelled as a percentage) fell below the plotted range.

For this experiment, we use a relatively compact Twincher model with approximately 2.5×10^4 trainable parameters. Training was performed in static-random mode using approximately 6.4×10^4 evaluations of the forward process. In Fig. 6, we visualize the state of the learned Twincher representation at the beginning and at the end of training by projecting the 2D manifolds $u(p)$ obtained by varying two components of p while fixing the remaining component to zero. One can observe that training leads to the formation of a smooth and regular representation that appears to be bijective over the evaluated range.

To evaluate the trained model, we generated 15 random hinge configurations within the specified parameter ranges and inferred the corresponding parameter vectors from noisy depth maps. The results are shown in Fig. 7, where true (red) and inferred (cyan) bounding rectangles and connection axes for both hinge components, as well as offset values, are overlaid. The model consistently recovers the underlying 3D structure despite substantial observation noise, while the noise causes reasonably small deviations from the underlying true states. We emphasize that these results were obtained using a comparatively small model with approximately 2.5×10^4 trainable parameters and should therefore be interpreted primarily as a proof-of-concept demonstration. Further improvements in robustness and invariance to noise are expected with increased model capacity and training time.

A notable property of the Twincher approach is that, under successful formation of a bijective representation, the inference errors can be attributed solely to noise or uncertainty in the observations y . To demonstrate this behavior, we generated random hinge configurations and applied observation noise with varying amplitudes. Figure 8 shows the resulting relationship between the RMS deviation Δp of the inferred parameters and the RMS perturbation Δy introduced in the observation space. The results exhibit a systematic empirically observed error bound of the form $\Delta p < \eta \Delta y$, with $\eta \approx 2.0$ over the evaluated range. We note that reducing η is directly aligned with the training objective of promoting invariance of the learned representation with respect to perturbations in y . In practice, the bound can be further tightened through increased model capacity and additional training.

Under the assumption that the test set is sufficiently large, the results suggest that the learned Twincher representation induces globally convergent iterative inverse inference under zero noise and provides controlled error bounds under noisy observations, thereby offering a potential route toward reliable operation and resilience to adversarially selected perturbations. Such behavior may appear atypical for trainable models, which are commonly viewed as statistical systems in which reducing errors is often associated with continuous expansion of the training dataset [1]. Nevertheless, the observed behavior of the proposed approach is structural in nature.

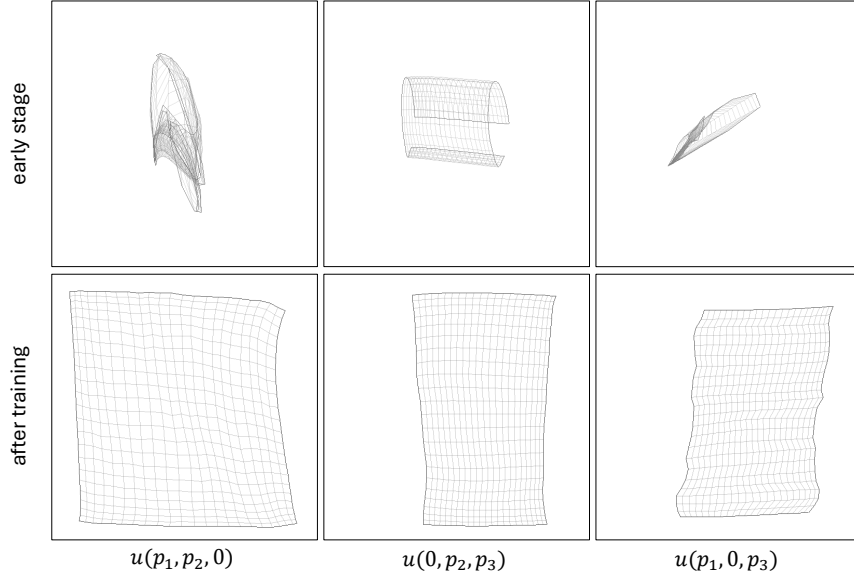


Figure 6: Projections of the 2D manifolds $u(p)$ obtained by fixing one component of p to zero and varying the remaining two over the interval $[-1, 1]$. The manifolds are projected onto the tangent plane at $p = 0$, spanned by the vectors Je_i and Je_k , where e_i and e_k denote canonical basis vectors in \mathcal{P} and $J = \partial u / \partial p|_{p=0}$. The upper and lower rows correspond to the Twincher representation at the beginning and at the end of training, respectively.

In the static training regime, the parameter space \mathcal{P} is sampled densely enough that the corresponding variations in y can be treated as locally smooth between sampled points, a property that can often be verified or estimated for practical forward processes. In the dynamic regime, the training process itself identifies regions of \mathcal{P} in which the forward mapping exhibits rapid variation, indicating where additional sampling is required. In both cases, training aims to construct a representation that captures sufficient information about the forward process to enable iterative inversion with controllable accuracy. From this perspective, the information encoded in the Twincher parameters can be interpreted as a compact representation of the forward process sufficient for stable inverse inference. Under this formulation, robustness to noise becomes a matter of enforcing invariance of the latent representation u with respect to perturbations in y , whether random or induced by a function describing model mismatch.

5 Conclusions

We have introduced Twincher, a class of architectures for learning bijective representations of continuous systems, together with the associated formulation of bijective representation learning. The proposed approach enables robust iterative inverse inference using learned bijective representation approximately invariant to noise and mismatch variations in the observation space.

Across synthetic benchmarks, we observe that the proposed approach can consistently improve data efficiency and robustness compared to standard inverse modeling baselines, particularly in regimes where sufficient exploration of the forward process is available. In this sense, the method provides a structured alternative to purely scaling-based approaches commonly associated with the compute-efficient frontier, by leveraging inductive bias and representation design rather than dataset or model scaling alone.

While the empirical results are limited to controlled synthetic settings, they suggest that explicitly enforcing bijective structure in learned representations may offer a useful principle for inverse problems. In particular, the resulting models appear to support stable inversion under moderate observation noise and enable error behavior that can be empirically bounded in practice.

More broadly, the proposed framework may serve as a modular component for learning-based systems in computer vision, robotics, and physical AI, where reliable inversion and controllable sensitivity to observation noise are important requirements. Future work includes scaling the approach to real-world systems, relaxing structural assumptions, and extending the framework to ill-posed inverse problems.

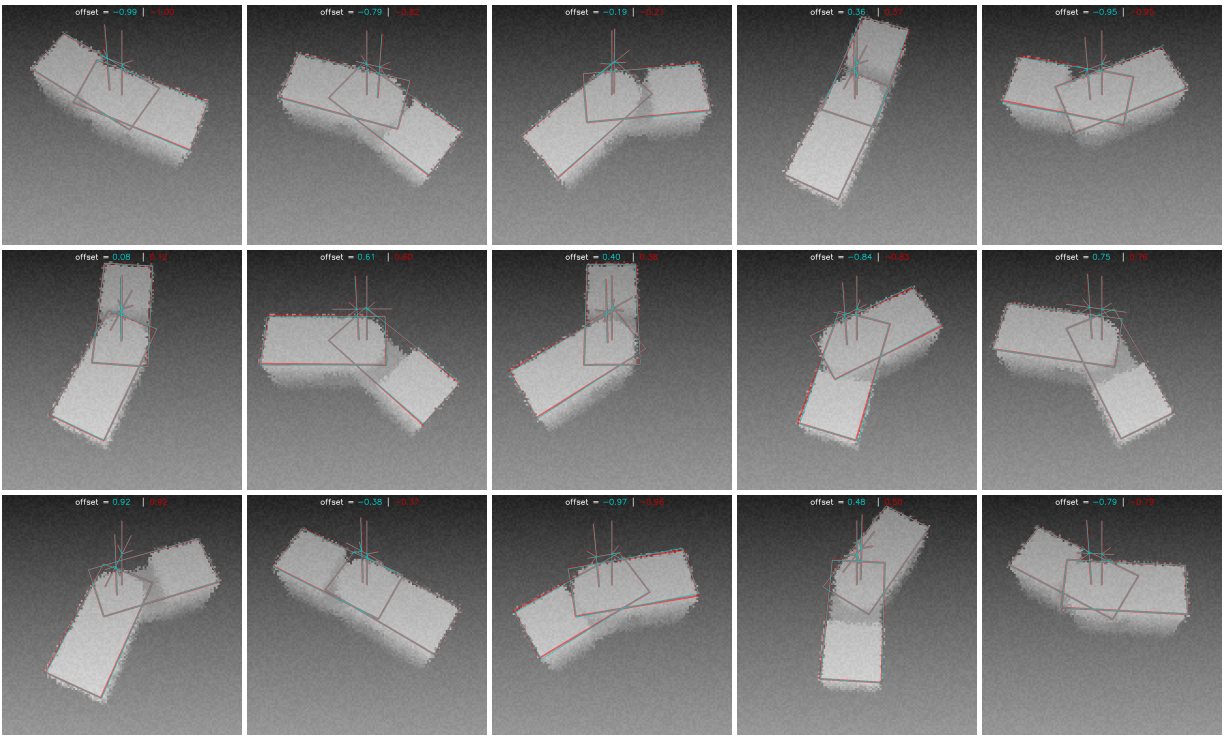


Figure 7: Fifteen randomly generated examples of 3D parameter inference using the trained Twincher model in the presence of observation noise. True (red) and inferred (cyan) bounding rectangles for both hinge components, connection axes, and offset values are shown.

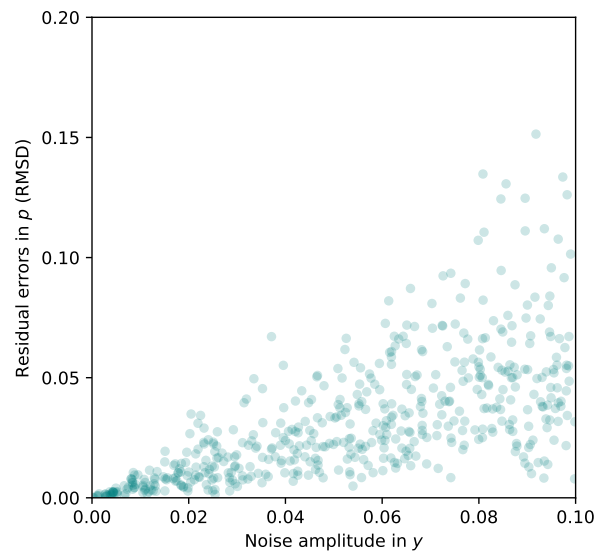


Figure 8: Dependence of the inference deviation from the true p vector (RMS) on the RMS perturbation magnitude in the observation space \mathcal{Y} for the Twincher model trained on the hinge reconstruction task.

References

- [1] Jared Kaplan, Sam McCandlish, Tom Henighan, Tom B Brown, Benjamin Chess, Rewon Child, Scott Gray, Alec Radford, Jeffrey Wu, and Dario Amodei. Scaling laws for neural language models. January 2020.
- [2] Y Lecun, L Bottou, Y Bengio, and P Haffner. Gradient-based learning applied to document recognition. *Proc. IEEE Inst. Electr. Electron. Eng.*, 86(11):2278–2324, 1998.
- [3] Ashish Vaswani, Noam Shazeer, Niki Parmar, Jakob Uszkoreit, Llion Jones, Aidan N. Gomez, Lukasz Kaiser, and Illia Polosukhin. Attention is all you need, 2017.
- [4] Alberto Bietti and Julien Mairal. On the inductive bias of neural tangent kernels, 2019.
- [5] Francesco Locatello, Stefan Bauer, Mario Lucic, Gunnar Rätsch, Sylvain Gelly, Bernhard Schölkopf, and Olivier Bachem. Challenging common assumptions in the unsupervised learning of disentangled representations. 2018.
- [6] David Ha and Jürgen Schmidhuber. World models. 2018.
- [7] Karl J Friston, Richard Rosch, Thomas Parr, Cathy Price, and Howard Bowman. Deep temporal models and active inference. *Neurosci. Biobehav. Rev.*, 90:486–501, July 2018.
- [8] Alexander A. Alemi, Ian Fischer, Joshua V. Dillon, and Kevin Murphy. Deep variational information bottleneck. 2016.
- [9] Ryo Sakagami, Florian S Lay, Andreas Dömel, Martin J Schuster, Alin Albu-Schäffer, and Freerk Stulp. Robotic world models-conceptualization, review, and engineering best practices. *Front. Robot. AI*, 10:1253049, November 2023.
- [10] Jingtao Ding, Yunke Zhang, Yu Shang, Jie Feng, Yuheng Zhang, Zefang Zong, Yuan Yuan, Hongyuan Su, Nian Li, Jinghua Piao, Yucheng Deng, Nicholas Sukiennik, Chen Gao, Fengli Xu, and Yong Li. Understanding world or predicting future? a comprehensive survey of world models, 2024.
- [11] Yanchen Guan, Haicheng Liao, Zhenning Li, Jia Hu, Runze Yuan, Yunjian Li, Guohui Zhang, and Chengzhong Xu. World models for autonomous driving: An initial survey, 2024.
- [12] Bohan Hou, Gen Li, Jindou Jia, Tuo An, Xinying Guo, Sicong Leng, Haoran Geng, Yanjie Ze, Tatsuya Harada, Philip Torr, Oier Mees, Marc Pollefeys, Zhuang Liu, Jiajun Wu, Pieter Abbeel, Jitendra Malik, Yilun Du, and Jianfei Yang. World model for robot learning: A comprehensive survey, 2026.
- [13] Thomas M Moerland, Joost Broekens, Aske Plaat, and Catholijn M Jonker. Model-based reinforcement learning: A survey. June 2020.
- [14] Aske Plaat, Walter Kusters, and Mike Preuss. High-accuracy model-based reinforcement learning, a survey. July 2021.
- [15] Xiaofeng Han, Shunpeng Chen, Zenghuang Fu, Zhe Feng, Lue Fan, Dong An, Changwei Wang, Li Guo, Weiliang Meng, Xiaopeng Zhang, Rongtao Xu, and Shibiao Xu. Multimodal fusion and vision–language models: A survey for robot vision. *Information Fusion*, 126:103652, 2026.
- [16] Kento Kawaharazuka, Jihoon Oh, Jun Yamada, Ingmar Posner, and Yuke Zhu. Vision-language-action models for robotics: A review towards real-world applications. *Techrxiv*, August 2025.
- [17] Rui Shao, Wei Li, Lingsen Zhang, Renshan Zhang, Zhiyang Liu, Ran Chen, and Liqiang Nie. Large VLM-based Vision-Language-Action models for robotic manipulation: A survey. September 2025.
- [18] Carlos Celemin, Rodrigo Pérez-Dattari, Eugenio Chisari, Giovanni Franzese, Leandro de Souza Rosa, Ravi Prakash, Zlatan Ajanović, Marta Ferraz, Abhinav Valada, and Jens Kober. Interactive imitation learning in robotics: A survey. October 2022.
- [19] Yuchen Wang, Mitsuhiro Hayashibe, and Dai Owaki. Data-driven policy learning methods from biological behavior: A systematic review. *Appl. Sci. (Basel)*, 14(10):4038, May 2024.
- [20] Rosa Wolf, Yitian Shi, Sheng Liu, and Rania Rayyes. Diffusion models for robotic manipulation: A survey. July 2025.
- [21] Jialong Li, Simon Kristoffersson Lind, Wenrui Xie, Maj Stenmark, and Volker Krüger. Normalizing flows are capable models for bi-manual visuomotor policy. February 2026.
- [22] Kieran A Murphy, Varun Jampani, Srikumar Ramalingam, and Ameesh Makadia. Learning ABCs: Approximate bijective correspondence for isolating factors of variation with weak supervision. March 2021.
- [23] Laurent Dinh, Jascha Sohl-Dickstein, and Samy Bengio. Density estimation using real NVP. May 2016.
- [24] Diederik P Kingma and Prafulla Dhariwal. Glow: Generative flow with invertible 1x1 convolutions. July 2018.

- [25] Ian J. Goodfellow, Jonathon Shlens, and Christian Szegedy. Explaining and harnessing adversarial examples, 2014.
- [26] Aleksander Madry, Aleksandar Makelov, Ludwig Schmidt, Dimitris Tsipras, and Adrian Vladu. Towards deep learning models resistant to adversarial attacks, 2017.
- [27] Hamed Rahimian and Sanjay Mehrotra. Distributionally robust optimization: A review. 2019.
- [28] Irina Higgins, Loic Matthey, Arka Pal, Christopher Burgess, Xavier Glorot, Matthew Botvinick, Shakir Mohamed, and Alexander Lerchner. beta-VAE: Learning basic visual concepts with a constrained variational framework. In *International Conference on Learning Representations*, 2017.
- [29] R Hadsell, S Chopra, and Y LeCun. Dimensionality reduction by learning an invariant mapping. In *2006 IEEE Computer Society Conference on Computer Vision and Pattern Recognition - Volume 2 (CVPR'06)*. IEEE, 2006.
- [30] Salah Rifai, Pascal Vincent, Xavier Muller, Xavier Glorot, and Yoshua Bengio. Contractive auto-encoders: explicit invariance during feature extraction. In *Proceedings of the 28th International Conference on International Conference on Machine Learning, ICML'11*, page 833–840, Madison, WI, USA, 2011. Omnipress.
- [31] Gaëtan Hadjeres, Frank Nielsen, and François Pachet. Glsr-vae: Geodesic latent space regularization for variational autoencoder architectures, 2017.
- [32] Georgios Arvanitidis, Lars Kai Hansen, and Søren Hauberg. Latent space oddity: on the curvature of deep generative models, 2017.
- [33] Ricky T. Q. Chen, Xuechen Li, Roger Grosse, and David Duvenaud. Isolating sources of disentanglement in variational autoencoders, 2018.
- [34] Hyunjik Kim and Andriy Mnih. Disentangling by factorising, 2018.
- [35] Jose Gallego-Posada and Patrick Forré. Simplicial regularization. In *ICLR 2021 Workshop on Geometrical and Topological Representation Learning*, 2021.
- [36] Marco Miani, Frederik Warburg, Pablo Moreno-Muñoz, Nicki Skafté, and Søren Hauberg. Laplacian autoencoders for learning stochastic representations. In S. Koyejo, S. Mohamed, A. Agarwal, D. Belgrave, K. Cho, and A. Oh, editors, *Advances in Neural Information Processing Systems*, volume 35, pages 21059–21072. Curran Associates, Inc., 2022.
- [37] Michael Rotman, Amit Dekel, Shir Gur, Yaron Oz, and Lior Wolf. Unsupervised disentanglement with tensor product representations on the torus, 2022.
- [38] Robin Rombach, Andreas Blattmann, Dominik Lorenz, Patrick Esser, and Björn Ommer. High-resolution image synthesis with latent diffusion models. December 2021.
- [39] Irina Higgins, Sébastien Racanière, and Danilo Rezende. Symmetry-based representations for artificial and biological general intelligence, 2022.
- [40] Vladislav Polianskii. An investigation of neural network structure with topological data analysis, 2018.
- [41] Theodoros Kouzelis, Ioannis Kakogeorgiou, Spyros Gidaris, and Nikos Komodakis. EQ-VAE: Equivariance regularized latent space for improved generative image modeling. In Aarti Singh, Maryam Fazel, Daniel Hsu, Simon Lacoste-Julien, Felix Berkenkamp, Tegan Maharaj, Kiri Wagstaff, and Jerry Zhu, editors, *Proceedings of the 42nd International Conference on Machine Learning*, volume 267 of *Proceedings of Machine Learning Research*, pages 31648–31666. PMLR, 13–19 Jul 2025.
- [42] Jose Gallego-Posada and Patrick Forré. Simplicial regularization. In *ICLR 2021 Workshop on Geometrical and Topological Representation Learning*, 2021.
- [43] Rickard Brüel Gabrielsson, Bradley J. Nelson, Anjan Dwaraknath, and Primoz Skraba. A topology layer for machine learning. In Silvia Chiappa and Roberto Calandra, editors, *Proceedings of the Twenty Third International Conference on Artificial Intelligence and Statistics*, volume 108 of *Proceedings of Machine Learning Research*, pages 1553–1563. PMLR, 26–28 Aug 2020.
- [44] Christoph Hofer, Roland Kwitt, Mandar Dixit, and Marc Niethammer. Connectivity-optimized representation learning via persistent homology. June 2019.
- [45] Aniss Aiman Medbouhi, Vladislav Polianskii, Anastasia Varava, and Danica Kragic. Invmap and witness simplicial variational auto-encoders. *Machine Learning and Knowledge Extraction*, 5(1):199–236, February 2023.
- [46] Helene Hauschultz, Rasmus Berg Palm Pablo Moreno-Muñoz, Nicki Skafté Detlefsen, Andrew Allan du Plessis, and Søren Hauberg. Is an encoder within reach? June 2022.
- [47] Ziming Liu, Yixuan Wang, Sachin Vaidya, Fabian Rühle, James Halverson, Marin Soljačić, Thomas Y Hou, and Max Tegmark. KAN: Kolmogorov-Arnold networks. April 2024.

- [48] Daniele Fakhoury, Emanuele Fakhoury, and Hendrik Speleers. ExSpliNet: An interpretable and expressive spline-based neural network. May 2022.
- [49] Seokhun Park, Insung Kong, Yongchan Choi, Chanmoo Park, and Yongdai Kim. Tensor product neural networks for functional ANOVA model. July 2025.
- [50] Oren Freifeld, Soren Hauberg, Kayhan Batmanghelich, and John W. Fisher, III. Highly-expressive spaces of well-behaved transformations: Keeping it simple. In *Proceedings of the IEEE International Conference on Computer Vision (ICCV)*, December 2015.
- [51] Laurent Dinh, David Krueger, and Yoshua Bengio. NICE: Non-linear independent components estimation. October 2014.
- [52] Twincher api for training and inference. <https://api.twincher.ai>. Proprietary API used for experimental reproduction. Documentation available upon request (contact@twincher.ai). Accessed: 2026-05-05.